Darcy's Law for Yield Stress Fluids

Chen Liu,[1,*] Andrea De Luca,[2,†] Alberto Rosso,[3,‡] and Laurent Talon[1,§]
[1]FAST, CNRS, Univ. Paris-Sud, Université Paris-Saclay, 91405 Orsay, France
[2]Theoretical Physics, Oxford University, Parks Road, Oxford OX1 3PU, United Kingdom
[3]LPTMS, CNRS, Univ. Paris-Sud, Université Paris-Saclay, 91405 Orsay, France

(Received 27 November 2018; published 21 June 2019)

Predicting the flow of non-Newtonian fluids in a porous structure is still a challenging issue due to the interplay between the microscopic disorder and the nonlinear rheology. In this Letter, we study the case of a yield stress fluid in a two-dimensional structure. Thanks to an efficient optimization algorithm, we show that the system undergoes a continuous phase transition in the behavior of the flow, controlled by the applied pressure difference. In analogy with studies of plastic depinning of vortex lattices in high-T_c superconductors, we characterize the nonlinearity of the flow curve and relate it to the change in the geometry of the open channels. In particular, close to the transition, a universal scale-free distribution of the channel length is observed and explained theoretically via a mapping to the Kardar-Parisi-Zhang equation.

DOI: 10.1103/PhysRevLett.122.245502

Introduction—Most of the water used for human consumption is stored in underground porous structures, called aquifers, where it is free to flow if a pressure difference P is applied. In 1852, H. Darcy [1] showed that the mean flow rate, Q, namely, the volume of fluid which passes per unit time measured in a region of size L, is proportional to the drop P/L: $Q = [(\kappa/\eta)(P/L)]$. Here η is the water viscosity and κ is the permeability, which depends on the composition of the porous structure. The permeability can vary many orders of magnitude: from the quite large values of fractured rock or gravel to the extremely small permeability of clay.

Darcy's law is not restricted to underground water, but is commonly used for oil, natural gas, and most Newtonian fluids embedded in a porous structure as long as the mean flow rate is small enough so that the inertia can be neglected [2–4]. However, it does not capture the behavior of many fluids currently injected in rocks for various applications. In hydraulic fracturing, for example, cracks induced by high-pressure fluid injection allow the flow of gas and oil [5]. The fracking fluids are emulsions of water and sand or other proppants needed to keep the paths open. Foams are used in the enhanced oil recovery to avoid the viscous fingering instability [6]. Complex fluids are also employed in soil consolidation by cement injection. All the aforementioned applications involve yield stress fluid, namely, liquids that are able to flow only above a finite yield stress, τ_y. Thus, it is an important question to understand how yield stress liquids flow in the ground and in general in porous materials [7–12]. Because of the yield stress property, flow occurs only above a critical pressure difference P_0. Because of the disorder, recent studies have shown that above this threshold the flow is characterized by a phase separation with regions that are easier to flow than others [11–13]. In this regime, the flow curve is nonlinear with $Q \propto (P - P_0)^\beta$ with $\beta > 1$. At higher pressure, linearity is recovered and the flow invades homogeneously in the material.

Interestingly, similar behaviors are observed in other disordered systems such as vortex lattices in high-Tc superconductor [14,15], skyrmions [16], or 2D colloidal crystals [17,18]. There, a *plastic depinning* is observed above a critical forcing, with vortices moving in preferential narrow channels and displaying a nonlinear flux with the applied force ($\beta > 1$). At larger force, a smectic ordered phase is observed and the flux becomes linear [19]. In all these systems, a dynamical continuous transition separates an arrested phase from a flowing one. In these conditions, universality and divergent correlation lengths are expected [20], but never proved even though power-law behavior has been reported in erosion models and experiments [21].

In this Letter, we provide a quantitative description of yield stress fluids in a stylized two-dimensional porous material. Introducing a very efficient optimization algorithm, we compute the flow curve of large systems without approximations and observe three distinct regimes. In particular, for the plastic flow, we find $Q \propto (P - P_0)^\beta$ with $\beta \simeq 2$. When $P \to P_0$, the distribution P_ℓ of channels of length ℓ becomes scale free: $P_\ell \propto 1/\ell$. A mapping with the model of directed polymer in random media allows us to show that this result is universal and belongs to the Kardar-Parisi-Zhang (KPZ) universality class [22].

The model.—The full solution of the flow through a porous medium is computationally costly even for Newtonian fluids, since it requires to solve the Navier-Stokes equations coupled with the no-slip condition at the complex solid interface. A significant simplification is provided by the pore network models [23] shown in

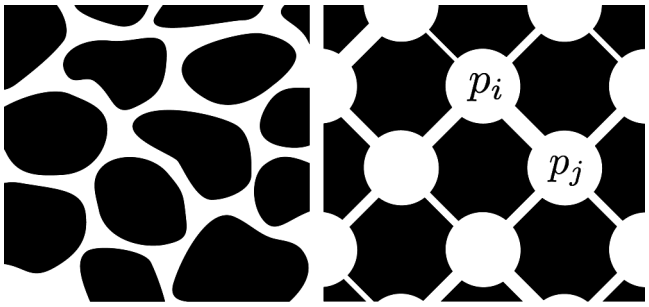

FIG. 1. Sketch of porous media. Left: realistic porous medium in which the solid phase consists of an assembly of grains (in black). Right: model of a pore network in which large open pores are connected by straight tubes (throats) with random radii and unit length.

Fig. 1. There the material is described by a lattice of large voids (the pores) connected by narrow cylindric tubes (the throats) of length l and radius r_0. In the pores the pressure is assumed homogeneous, the flow occurs in the throats where it can be computed even for a yield stress fluid. In particular for a Bingham rheology [24], the local flow rate in the throat connecting the pores i and j writes

$$q_{ij} = \begin{cases} \sigma_{ij}(\Delta p_{ij} - \tau_{ij}) & \text{if: } \Delta p_{ij} > \tau_{ij} \\ 0 & \text{if: } |\Delta p_{ij}| < \tau_{ij}\,, \\ \sigma_{ij}(\Delta p_{ij} + \tau_{ij}) & \text{if: } \Delta p_{ij} < -\tau_{ij} \end{cases} \quad (1)$$

with the local pressure difference $\Delta p_{ij} = p_i - p_j$. For cylindric throat of length l and radius r_0, according to the Poiseuille law [25,26], the local hydraulic conductivity $\sigma_{ij} \sim r_0^4/l$ and the local pressure threshold $\tau_{ij} = \tau_y l/r_0$. For simplicity, we set $l = 1$ and r_0 random, as a consequence both local conductivities and thresholds are random.

Equation (1) should be combined with the Kirchhoff's conservation of the flow at each node $\sum_{j\in n(i)} q_{ij} = 0$, where the sum runs over the set $n(i)$ of neighbors of the node i. This conservation holds for all nodes except the inlet node (see Fig. 2 left) where the fluid is injected at pressure P and the outlet node where the fluid is evacuated at zero pressure. Given the total pressure difference P and the configuration of random thresholds and conductivities, Eq. (1) together with Kirchhoff's condition is closed, but very difficult to solve due to the nonlinearity of the flow rate function of Eq. (1).

To resolve this task, we developed a method based on the observation that, for a given pressure difference, the flow occurs only in the set of open throats, named $\mathcal{L}(P)$. Once $\mathcal{L}(P)$ is known, the solution of the local pressure becomes linear and can be written as $p_i = a_i P + b_i$, where the coefficients a_i, b_i depend on $\mathcal{L}(P)$ and their expressions are given in the Supplemental Material [27]. The set of open throats, $\mathcal{L}(P)$, is determined iteratively starting from the minimal pressure P_0 needed to open the first channel connecting the inlet and the outlet pores. P_0 is obtained by minimizing

$$P_0 = \min_{C\in\mathcal{C}_{\text{in-out}}} \sum_{(ij)\in C} \tau_{ij}, \quad (2)$$

where $\mathcal{C}_{\text{in-out}}$ represents the set of all paths connecting the inlet and outlet nodes. The channel C_0 corresponds to the path that realizes the minimum so that $\mathcal{L}(P_0) = C_0$. For slightly larger pressure, the flow remains restricted to this channel and thus $\mathcal{L}(P) = \mathcal{L}(P_0)$. Increasing the pressure, $\mathcal{L}(P)$ is enlarged as new channels will open. The changes of $\mathcal{L}(P)$ are the manifestation of the nonlinearity of the problem and, for a given realization of the thresholds, occur at precise pressure values $P_0 < P_1 < P_2 < \ldots$ as shown in Fig. 2. In order to determine P_k, and the corresponding $\mathcal{L}(P_k)$, knowing $\mathcal{L}(P_{k-1})$, we should consider the set A_{k-1} of all pairs of active nodes belonging to $\mathcal{L}(P_{k-1})$. For each node pair $(n, m) \in A_{k-1}$, we consider the set $\mathcal{C}_{mn}$ of all paths that connect n and m and that avoid any other intersection with $\mathcal{L}(P_{k-1})$ beyond the end points. The optimal path among $\mathcal{C}_{mn}$ has a threshold

$$E_{mn} = \min_{C\in\mathcal{C}_{mn}} \sum_{(ij)\in C} \tau_{ij}. \quad (3)$$

For a given $P > P_{k-1}$, if, for all pairs of nodes $(m, n) \in A_{k-1}$, the threshold E_{mn} is larger than the corresponding pressure difference $\Delta p_{mn}(P)$, then no new channels appear and $\mathcal{L}(P) = \mathcal{L}(P_{k-1})$. Expressing p_m and p_n in terms of a_m, b_m and a_n, b_n respectively, the pressure P_k is then determined by

$$P_k = \min_{(m,n)\in A_{k-1}} \frac{E_{mn} - (b_m - b_n)}{a_m - a_n}. \quad (4)$$

The minimizations of Eqs. (2) and (3) are performed using the Dijkstra optimization algorithm [28] which is quadratic in the path length. In principle, the channel can be nondirected, i.e., can involve throats where the flow is upward, but in practice the statistics is dominated by the directed ones [13,29] and for simplicity we restrict our analysis to them.

Once the local pressures p_i are known, the total flow Q is given by the outgoing flow from the inlet node. In particular in our model, the flow curve reads $Q(P) = \kappa_k(P - P_{k-1})/L + Q(P_{k-1})$ if $P_{k-1} < P < P_k$, where κ_k is the permeability of the set $\mathcal{L}(P_{k-1})$.

Results.—For the sake of simplicity, here we discuss the case $\sigma_{ij} = 1$. In Ref. [27], our study is extended to fluctuating local conductivities and the main results are shown to be totally universal. The flow curve [Fig. 3(a)] shows two linear regimes at low and high pressures: close to P_0 the permeability is $\kappa_1 = 1$ while, at very large pressure, it converges to the Newtonian value ($\tau_{ij} = 0$):

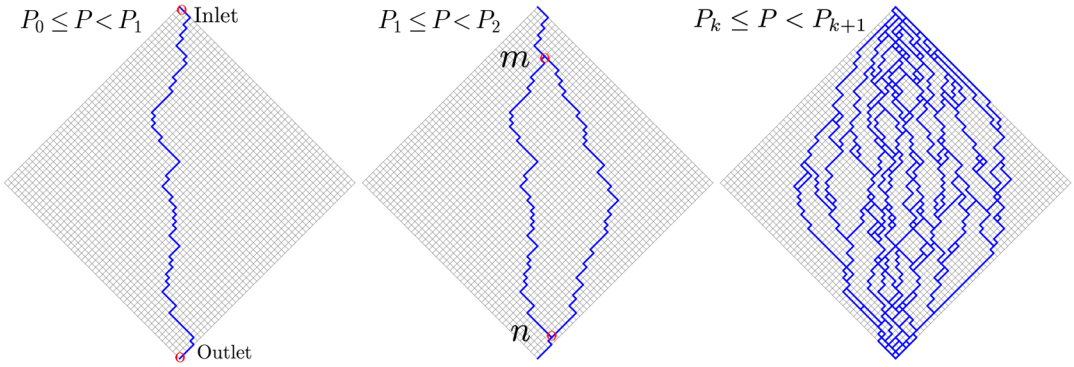

FIG. 2. The flowing path network at different applied pressures for a system of size $L = 100$.

$\kappa_\infty \sim \pi L/(4 \log L)$ (see Ref. [27] for the derivation of this result and for the numerical evidences) with a total flow: $Q(P) = (\kappa_\infty P - \sum_{ij} \tau_{ij})/L$.

The regime at intermediate pressure is extremely interesting: it is characterized by a complex geometry of open channels [Fig. 2(c)] and by a nonlinear growth of the flow rate [Fig. 3(a)]. A power-law behavior emerges with an exponent β close to 2. The origin of this nonlinearity comes from the opening of new channels which increases the permeability [as shown in the inset of Fig. 3(a)]. Indeed, in Fig. 3(b), we study the sequence of pressure gaps $\Delta P_k \equiv P_k - P_{k-1}$ and the permeability κ_k as a function of the number of open paths k. Independently of the threshold distribution, a clear power-law behavior is observed and we can conclude that the number of open paths grows quadratically with $P - P_0$ (i.e., $P - P_0 = \sum_k \Delta P_k \sim \int dk k^{-1/2} \sim k^{1/2}$), while the permeability $\kappa_k \simeq k^{1/2}$, which implies $Q = \frac{1}{L}\sum_{k'=1}^{k} \kappa_{k'} \Delta P_{k'} \sim k$ in agreement with $\beta = 2$. The value of the exponent seems then to be independent on the threshold distribution (see also the Supplemental Material [27]) and is also in agreement with the one found by solving the full Bingham rheology problem in realistic porous structures (e.g., random beads packing [11,13]). This suggests that the macroscopic rheology might be universal and that the system approaching P_0 is undergoing a dynamical second-order phase transition. To assess this idea, we then search for fingerprints of criticality and scale-free behavior.

In particular, we can provide a deeper understanding on how the nonlinearity of the flow is approached from small P. In the inset of Fig. 3(a), we present the flow curve for a single realization for $P \gtrsim P_0$. The exact linearity terminates at $P = P_1$ when a second path opens. In this case, Eq. (4) can be simplified to

$$P_1 = P_0 + L \min_{(m,n)\in\mathcal{L}(P_0)} \left(\frac{\delta E_{mn}}{\ell_{mn}} \right), \tag{5}$$

where ℓ_{mn} is the distance between m and n and $\delta E_{mn} = E_{mn} - E^0_{mn}$, with E^0_{mn} the threshold along C_0 between n and m. The presence of the second path C_1 induces a change on the permeability that depends on the length ℓ of C_1. In particular, one has $\kappa_2 = [L/L - (\ell/2)]$. Note that, depending on the size of the reorganization ℓ, the permeability can increase up to a factor 2 for $\ell \sim L$.

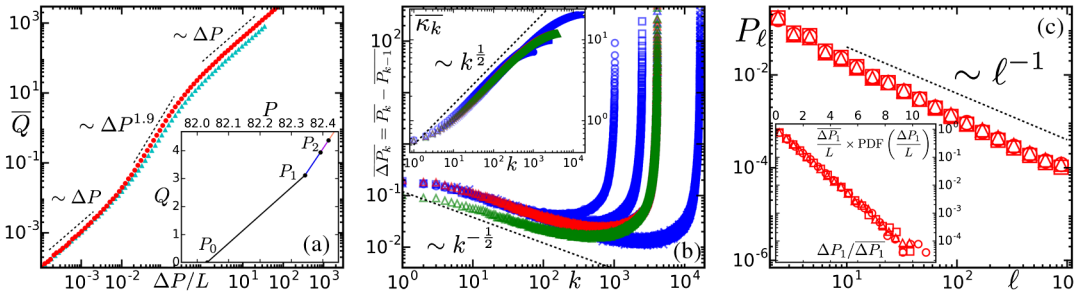

FIG. 3. (a) The mean flow curve $\bar{Q}$ for a given $\Delta P = P - P_0$ averaged over more than 200 realizations. The thresholds τ_{ij} are uniformly distributed in $[2 - \sqrt{3}/5, 2 + \sqrt{3}/5]$. Circles and triangles correspond to $L = 64$ and $L = 128$, respectively. Inset: the flow curve of a single realization ($L = 50$). (b) The averaged pressure increments $\overline{\Delta P_k}$ as function of number of open paths k. Inset: the averaged permeability $\overline{\kappa_k}$ as function of the number of open paths k. Circles, squares, triangles, and crosses correspond to different system sizes $L = 64$, 100, 128, 256; blue, red, green correspond to different threshold distributions respectively: uniform, Gaussian, exponential. (c) The PDF of lengths of the second open paths P_ℓ. Inset: the PDFs of gaps for different system sizes renormalized by their mean values which follow a clear exponential distribution. ○, □, and △ correspond to different threshold distributions: uniform, Gaussian, and exponential, respectively.

Remarkably as shown in Fig. 3, the statistics of the reorganization size is a power law decaying as $P(\ell) \propto 1/\ell$, which characterizes a scale-free behavior. We can explain this result by using a mapping with the directed polymer in random media and its connection with the KPZ universality class [22,30,31].

Directed polymers and KPZ.—The minimization problem in Eq. (2) is equivalent to finding the ground state of a directed polymer (DP) of length L in $(1+1)$d random medium and the pressure P_0 corresponds to its energy [22]. DP is a well-known model that belongs to the KPZ universality class and the sample-to-sample fluctuations of the ground state energy have been largely studied in the literature: they display an anomalous scaling $\propto L^{\theta}$ where the exponent θ is characteristic of the KPZ universality class. In $(1+1)$d, not only the exact value $\theta = 1/3$ is known [22,30,32], but all the fluctuations of the ground state energy are universal and governed by Tracy-Widom distribution [33]. The second path that opens at P_1 can be seen as an excited state, on which much less is known. It is natural to expect that the *constraint* of avoiding the ground state along the segment delimited by (n, m) produces a gap value that grows with the reorganization length ℓ_{mn}. Scaling arguments suggest that the same exponent θ controls its scaling, i.e., $\delta E_{mn} \propto \ell_{mn}^{1/3}$ [34]. If this scaling form is plugged in Eq. (5), one obtains the saturation of the typical size of the reorganization $\ell \simeq L$ and a gap growth $P_1 - P_0 \propto L^{1/3}$. Note that if in Eq. (5), one takes the factor $1/\ell_{mn}$ out of the minimization, the same argument would lead to a typical reorganization size of $\ell \simeq 1$ and to $P_1 - P_0 \propto L$. The numerical results obtained using our exact construction totally disagree with these predictions: ℓ displays a beautiful scale-free behavior [Fig. 3(c)], and $P_1 - P_0$ shrinks to zero logarithmically with the system size L (see Fig. 5 in Ref. [27]).

This suggests that, while the typical gaps scale as $\ell_{mn}^{1/3}$, those which realize the minimum in Eq. (5) are the results of rare paths. These rare, almost vanishing, gaps are the ones that determine P_1. To be more quantitative, we study in Ref. [27] (see also references in there [35–38]) the full PDF of δE_{mn} [denoted by $\rho_{\ell_{mn}}(\delta E_{mn})$] and show that

$$\rho_{\ell_{mn}}(\delta E_{mn} \to 0) \sim \frac{1}{\ell_{mn}}, \tag{6}$$

(see Fig. 7 of Ref. [27]) [39]. Note that this result is not only a numerical observation, but it is the consequence of an exact result: the probability to find almost degenerate self-avoiding ground states is inversely proportional to the polymer length [36,37].

We can prove the main results of the gap and length statistics of the second path in two steps.

First step: Consider all pairs of node (m, n) with a given distance $\ell_{mn} = \ell$ and select the excitation with the minimal cost among them: $\delta e_\ell = \min_{\ell_{mn}=\ell} \delta E_{mn}$. Note that δe_ℓ is the minimum among $L - \ell$ random variables that are identically distributed but display strong correlations, as the ground states of close pairs [e.g., $(n, n+\ell)$ and $(n+1, n+\ell+1)$] have large overlaps. It is reasonable to assume that the effective number of independent variables scales as the number of nonoverlapping blocks $N_\ell = L/\ell$ and the statistics of δe_ℓ is the minimum among them. From Eq. (6), for large N_ℓ, we have

$$\begin{aligned} \text{Proba}[\delta e_\ell > x] &= \left[1 - \int_0^x d(\delta E)\rho_\ell(\delta E)\right]^{N_\ell} \\ &\approx \exp\left[-N_\ell \int_0^x d(\delta E)\rho_\ell(\delta E)\right] \\ &\approx \exp\left(-\frac{N_\ell}{\ell} x\right). \end{aligned} \tag{7}$$

Second step: To have access to ΔP_1, we take into account all lengths $\ell = 2, 3 \ldots L$ to minimize the energy cost per length.

$$\frac{\Delta P_1}{L} = \min_\ell \frac{\delta e_\ell}{\ell} \tag{8}$$

Hence, using Eq. (7), we have

$$\begin{aligned} \text{Proba}\left(\frac{\Delta P_1}{L} > x\right) &= \prod_{\ell=2}^{L} \text{Proba}\left[\frac{\delta e_\ell}{\ell} > x\right] \\ &\approx \prod_{\ell=2}^{L} \exp(-N_\ell x) \\ &= \exp\left[-\left(\sum_{\ell=2}^{L} N_\ell\right) x\right] \end{aligned} \tag{9}$$

Thus, the gap $\Delta P_1/L$ is also exponentially distributed as shown in the inset of Fig. 3(c). Its mean, $\overline{\Delta P}_1/L = (\sum_\ell N_\ell)^{-1} \sim 1/[L \log(L/2)]$, is in agreement with the numerical results reported in Ref. [27] [see Fig. 5(b) therein]. Moreover, discarding the factor $1/\ell_{mn}$ in the minimization of Eq. (8), one recovers the mean $[\sum_\ell (N_\ell/\ell)]^{-1} \sim L^{-1}$ reported in Ref. [27].

Finally, to compute the statistics of the size of the second path P_ℓ, it is useful to introduce $\omega_\ell = \delta e_\ell/\ell$, take the derivative of Eq. (7) and obtain the PDF of ω_ℓ

$$p_\ell(\omega_\ell) \approx N_\ell \exp(-N_\ell \omega_\ell), \tag{10}$$

then the probability P_ℓ writes

$$P_\ell = \int d\omega_\ell p_\ell(\omega_\ell) \prod_{\ell' \neq \ell} \int_{\omega_\ell}^{\infty} p_{\ell'}(\omega_{\ell'}) \sim \ell^{-1}, \tag{11}$$

which is coherent with our observations for all types of distributions of thresholds shown by the red curves in

Fig. 3(c). Similarly, if one discards the factor $1/\ell$ in the minimization, one obtains the length distribution scales as ℓ^{-2} [Fig. 3 in Ref. [27]].

Conclusions.—In this Letter, we have studied the nonlinearity of the Darcy's law for a yield stress fluid in a 2D porous material. We have shown that the onset of flow is associated to a plastic depinning transition. In this context, power-law behaviors have been found [21] but here, we clearly identify a divergent scale in the length of the new channels. Our results are independent of the threshold distributions suggesting that in 2D geometry our main predictions $\beta \approx 2$ and $P_\ell \sim \ell^{-1}$ should be experimentally observed. It would be interesting to study the fractal properties of the flowing region (exact results have been obtained for the geometry of the branching paths of the first passage percolation model relevant for delta rivers [40] and animal trails [41]) and connect them to the value of the exponent β.

We expect the method developed here to be generalizable to 3D where the value of β is not known, but the statistics of P_ℓ will once again depend only on the scaling behavior of $\rho_\ell(\delta E \to 0)$.

This work is supported by "Investissement d'Avenir" LabEx PALM (Grant No. ANR-10-LABX-0039-PALM) and by the European Union's Horizon 2020 research and innovation programme under the Marie Sklodowska-Curie Grant No. 794750 (A. D. L.).

*chen.liu@u-psud.fr
†andrea.deluca@physics.ox.ac.uk
‡alberto.rosso@u-psud.fr
§laurent.talon@u-psud.fr

[1] H. Darcy, *Les fontaines publiques de la ville de Dijon. Exposition et application des principes à suivre et des formules à employer dans les questions de distribution d'eau* (Victor Dalmont, Paris, 1856).
[2] P. Forchheimer, Z. Ver. Deutsch, Ing. **45**, 1782 (1901).
[3] C. C. Mei and J.-L. Auriault, J. Fluid Mech. **222**, 647 (1991).
[4] S. Whitaker, Transp. Porous Media **25**, 27 (1996).
[5] A. C. Barbati, J. Desroches, A. Robisson, and G. H. McKinley, Annu. Rev. Chem. Biomol. Eng. **7**, 415 (2016).
[6] J. Nittmann, G. Daccord, and H. E. Stanley, Nature (London) **314**, 141 (1985).
[7] V. Entov, Prikl. Mat. Mekh. **31**, 820 (1967).
[8] T. Al-Fariss and K. L. Pinder, Can. J. Chem. Eng. **65**, 391 (1987).
[9] L. Talon and D. Bauer, Eur. Phys. J. E **36**, 139 (2013).
[10] T. Chevalier, C. Chevalier, X. Clain, J. Dupla, J. Canou, S. Rodts, and P. Coussot, J. Non-Newtonian Fluid Mech. **195**, 57 (2013).
[11] T. Chevalier and L. Talon, Phys. Rev. E **91**, 023011 (2015).
[12] T. Chevalier and L. Talon, Eur. Phys. J. E **38**, 76 (2015).
[13] L. Talon, H. Auradou, M. Pessel, and A. Hansen, Europhys. Lett. **103**, 30003 (2013).
[14] F. Pardo, F. De La Cruz, P. Gammel, E. Bucher, and D. Bishop, Nature (London) **396**, 348 (1998).
[15] A. B. Kolton, D. Domínguez, and N. Grønbech-Jensen, Phys. Rev. Lett. **83**, 3061 (1999).
[16] C. Reichhardt, D. Ray, and C. J. Olson Reichhardt, Phys. Rev. Lett. **114**, 217202 (2015).
[17] C. Reichhardt and C. J. Olson, Phys. Rev. Lett. **89**, 078301 (2002).
[18] A. Pertsinidis and X. S. Ling, Phys. Rev. Lett. **100**, 028303 (2008).
[19] C. Reichhardt and C. O. Reichhardt, Rep. Prog. Phys. **80**, 026501 (2017).
[20] J. Watson and D. S. Fisher, Phys. Rev. B **54**, 938 (1996).
[21] P. Aussillous, Z. Zou, É. Guazzelli, L. Yan, and M. Wyart, Proc. Natl Acad. Sci. U.S.A. **113**, 11788 (2016).
[22] M. Kardar, G. Parisi, and Y. C. Zhang, Phys. Rev. Lett. **56**, 889 (1986).
[23] I. Fatt *et al.*, AIME **207**, 144 (1956).
[24] E. C. Bingham, *Fluidity and Plasticity* (McGraw-Hill, New York, 1922), Vol. 2.
[25] R. B. Bird, R. C. Armstrong, and O. Hassager, *Dynamics of Polymeric Liquids* (John Wiley and Sons Inc, New York, 1987), Vol. 1.
[26] L. Talon, H. Auradou, and A. Hansen, Front. Phys. **2**, 24 (2014).
[27] See Supplemental Material at http://link.aps.org/supplemental/10.1103/PhysRevLett.122.245502 for the computing method, data supporting the universality of our results and a detailed discussion on the first energy gap distribution.
[28] E. W. Dijkstra, Numer. Math. **1**, 269 (1959).
[29] A. Hansen and J. Kertész, Phys. Rev. Lett. **93**, 040601 (2004).
[30] M. Kardar and Y.-C. Zhang, Phys. Rev. Lett. **58**, 2087 (1987).
[31] S. Roux and H. J. Herrmann, Europhys. Lett. **4**, 1227 (1987).
[32] D. A. Huse and C. L. Henley, Phys. Rev. Lett. **54**, 2708 (1985).
[33] K. Johansson, Commun. Math. Phys. **209**, 437 (2000).
[34] T. Hwa and D. S. Fisher, Phys. Rev. B **49**, 3136 (1994).
[35] C. Greene, Adv. Math. **14**, 254 (1974).
[36] A. De Luca and P. Le Doussal, Phys. Rev. E **92**, 040102(R) (2015).
[37] A. De Luca and P. Le Doussal, Phys. Rev. E **93**, 032118 (2016).
[38] A. De Luca and P. Le Doussal, Phys. Rev. E **95**, 030103(R) (2017).
[39] The Supplemental Material shows that these rare degenerate ground states correspond to polymers that are spatially well separated. In this limit, the repulsion between the two polymer configurations is very weak and very small gaps can be observed.
[40] G. Barraquand and M. Rychnovsky, arXiv:1807.01824.
[41] K. Kawagoe, G. Huber, M. Pradas, M. Wilkinson, A. Pumir, and E. Ben-Naim, Phys. Rev. E **96**, 012142 (2017).